Langmuir

ARTICLE

pubs.acs.org/Langmuir

Effect of Electric Field on Liquid Infiltration into Hydrophobic Nanopores

Baoxing Xu,[†] Yu Qiao,[‡] Qulan Zhou,[§] and Xi Chen[†,⊥,∥,*]

[†]Columbia Nanomechanics Research Center, Department of Earth and Environmental Engineering, Columbia University, New York, New York 10027, United States

[‡]Department of Structural Engineering, University of California—San Diego, La Jolla, California 92093-0085, United States

[§]State Key Laboratory of Multiphase Flow in Power Engineering, Xi'an Jiaotong University, Xi'an 710049, China

[⊥]School of Aerospace, Xi'an Jiaotong University, Xi'an 710049, China

[∥]Department of Civil & Environmental Engineering, Hanyang University, Seoul, 133-791, Korea

ABSTRACT: Understanding the variation of nanofluidic behavior in the presence of an external electric field is critical for controlling and designing nanofluidic devices. By studying the critical infiltration pressure of liquids into hydrophobic nanopores using molecular dynamics (MD) simulations and experiments, important insights can be gained on the variation of the effective liquid−solid interfacial tension with the magnitude and sign of electric field, as well as its coupling with the pore size and the solid and liquid species. It is found that the effective hydrophobicity reduces with the increase of electric intensity and/or pore size, and the behavior is asymmetric with respect to the direction of the electric field. The underlying molecular mechanisms are revealed via the study of the density profile, contact angle, and surface tension of confined liquid molecules.

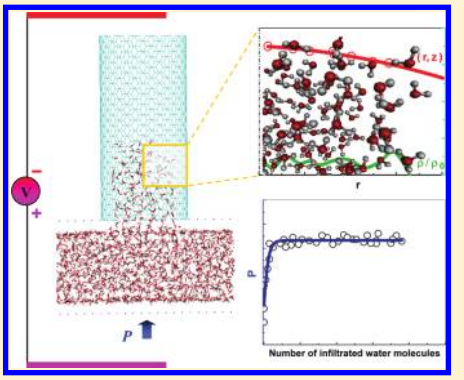

INTRODUCTION

In a confined nanoenvironment, owing to the unique solid−liquid interfacial characteristics, the liquid infiltration and transport exhibit many interesting phenomena.[1−3] Nanotubes can be spontaneously filled with liquids only when the surface tension of the liquid is low enough to allow internal wetting.[4] Otherwise, an external pressure is required to force a nonwetting liquid to infiltrate a hydrophobic nanoporous material, and during this process, the external work will be in part converted to solid−liquid interfacial tension and in part dissipated via friction during nanofluidic transport.[5] The performance of such a nanoporous energy absorption system (NEAS) is critically affected by the infiltration pressure[6] (at which the capillary resistance of the nanopore walls is overcome), which can be adjusted by tuning the effective hydrophobicity of the system. Several strategies have been proposed to control the nanofluidic infiltration and flow behavior by modifying the solid−liquid interfacial characteristics, such as adjusting the nanopore structure,[7] surface treatment,[8] adding the gas[9] or ion[10] phase, and/or applying an external pressure,[11] thermal field,[12] or electric field.[13] Among these approaches, the electrical control is in particular attractive because it is relatively simple and straightforward, maintains the inherent characteristics of nanopores such as their mechanical strength and surface morphology, while affecting the nanofluidic behavior by influencing the configurations of polar liquid molecules in nanoenvironment. Note that although the employment of static charge groups (by introducing explicit electric charges near a nanopore) may trigger and speed up flow or infiltration of liquids, it cannot drive a continuous flow of water molecules through a nanopore.[14,15]

In the presence of an external electric field, because of its dipole and quadrupole moments, water molecules feature strong interactions with the electric field next to the charged or polar solutes, and they are attracted to the field exposed regions, which may affect the effective surface tension of water molecules on nanopore wall,[16,17] also known as the electrocapillary effect. Garate simulated water-self-diffusion through single-walled carbon nanotubes (CNTs) using molecular dynamics (MD) simulations in the presence of an external electric field,[18] and found that the permeation of water into the smaller nanotubes is enhanced by electric fields due to a decrease in the fluctuations of the number of water molecules inside the nanotubes, whereas the larger extent of rotational freedom of the water molecules in the larger nanotubes allows an improved dipole alignment with the electric fields, resulting in a reduced water self-diffusion flux. By imposing an external voltage to a NEAS consists of nanoporous silica in KCl solution, Lu et al. found that the interfacial tension decreases as the applied voltage increases, and the

Received: February 4, 2011
Revised: April 5, 2011
Published: April 14, 2011

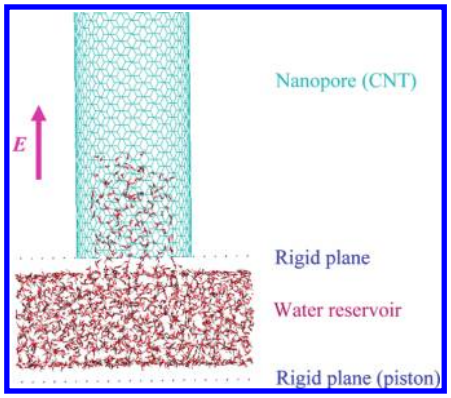

Figure 1. Computational cell of the model water/CNT system: One end of a carbon nanotube (CNT) is inserted into a water reservoir; the CNT is sufficiently long so that no water molecule will flow out from the other end during simulations. Pressure is applied through the piston-like bottom plane of the reservoir. The loading is quasi-static. A periodical boundary condition is imposed to the four lateral planes of the cell. An external electric field, E, is applied in the cell along the length direction of CNT (the current direction is positive).

magnitude of such a variation is smaller than its bulk counterpart.[13] Despite these preliminary investigations, the role of the electric field on the solid−liquid interfacial tension in a confining nanoenvironment remains unclear. Through the exploration of the performance variation of a NEAS under different electrical fields, in particular the infiltration pressure (which is closely related to the capillary resistance), the goal of the present paper is to obtain some useful insights on the effect of voltage on the solid−liquid interfacial tension. In turn, such a study may be helpful for designing electrically controllable NEAS or electrical actuation system through the adjustment of the relative hydrophobicity of nanoporous solid/functional liquid systems.

Using MD simulations, in this paper, we study the infiltration of liquid molecules into nanopores in the presence of an external electric field, in particular the dependency of the NEAS infiltration pressure on the external electric field and pore size. Both liquid and solid phases are varied: the working fluid includes water and electrolyte, and both carbon and silica nanotubes are taken as model nanochannels, so that the different influences of electric field can be revealed. The contact angle, surface tension, and liquid distribution density are employed to describe the solid−liquid interfacial characteristics. Parallel experiment is carried out on a similar system to justify the theoretical predictions. The results may be helpful for developing prospective electrically controllable nanofluidic protection and actuation devices.

MODEL AND COMPUTATIONAL METHOD

The computational cell is sketched in Figure 1. In this representative system, a model structure of nanochannel, an armchair (16,16) CNT with the diameter of 2.17 nm,[19] has one of its openings immersed in a reservoir filled with model nonwetting liquid, which contains 2548 water molecules. The nanopore size and phase, as well as the liquid phase, are varied later in this study. The nanotube is assumed to be rigid and previous studies[20] have indicated that the effect of tube flexibility is minor. The top and bottom surfaces of the reservoir are bounded by two rigid planes, with the upper one fixed and the lower one movable to mimic a piston. Initially, the averaged density of water in the reservoir is close to that of bulk water, ρ_0 = 998.0 kg/m^3 at 300 K and 0.1 MPa by adjusting the total number of water molecules. A periodical boundary condition is imposed on the four lateral planes of the computational cell.

MD simulation is performed using LAMMPS (large-scale atomic/molecular massively parallel simulator), with the NVT ensemble at ambient temperature of 300 K.[21,22] The nonbond interatomic van der Waals interaction is described by the 12−6 Lennard-Jones (LJ) empirical forcefield, $U(r_{ij}) = 4\varepsilon[(\sigma/r_{ij})^{12} - (\sigma/r_{ij})^6]$, where r_{ij} denotes the distance between atoms, and ε and σ are the energy and length parameters, respectively. In the example CNT−water system described in Figure 1, due to the lack of available flexible water model for reproducing all behaviors of water deformation (e.g., oxygen−hydrogen bond, bond angle and bending frequency)[23] when subjected to an electric field,[24] the water is modeled by the most popular force fields of the extended simple point charge potential (SPC/E).[25] The particle−particle particle−mesh (PPPM) technique with a root-mean-square accuracy of 10^{-4} is employed to handle the long-range Coulomb interactions between the sites associated with the oxygen atoms and the two hydrogen atoms. The carbon−oxygen LJ parameters are extracted from the experimental low-coverage isotherm data of oxygen adsorption on graphite.[26,27] By using these molecular models and parameters, the graphene as the raw material for constructing CNTs is ensured to be hydrophobic[28] in the absence of electric field; with the application of an external electric field, as will be shown below, the hydrophobility will decrease; nevertheless, the system will not switch to hydrophilic. When the solid and liquid phases are changed, e.g., with the employment of silica nanotube and electrolyte, relevant force field parameters can be found in refs.[11,29,30]

Since the inner surface of nanotube is hydrophobic, after equilibrium the water molecules cannot enter into the nanotube spontaneously. By moving the piston upward in a quasi-static manner,[31] the water phase is pressurized. At each time step, the effective applied pressure, P, is evaluated by sampling a region with volume of V near the entrance of the nanotube, based on the intermolecular potential among water molecules via the Virial expression, $P = N'k_BT/V + \Sigma_i^{N'} r_i \cdot f_i/3V$,[32] where N' is the number of water molecules inside the sampling region, k_B is the Boltzmann constant, T is the system temperature, and the second term describes the contribution from the pair wise body interaction among the N' water molecules. V is taken to be sufficiently large to ensure a nearly isotropic density distribution of water. If the pressure is beyond a critical infiltration value, P_{in}, liquid starts to infiltrate and wet the nanopore.

A uniform external electric field, E, is applied along the axial direction of the nanochannel, whose magnitude varies between 10^{-2} V/Å < $|E|$ < 0.4 V/Å, which is on the same order of that for ion channels and membranes,[33,34] and the results are compared with the reference system without electric field. Note that the applied electric field in this study does not include the field reduction due to water polarization, and this assumption has been rationalized for the SPC/E water model.[17,35]

RESULTS AND DISCUSSION

Infiltration Characteristics and Pore Size Dependence of Reference System. We first explore the fundamental behavior of the reference system, by studying the infiltration of water molecules into a representative (16,16) CNT without an external electric field. Figure 2 shows the variation of the number of

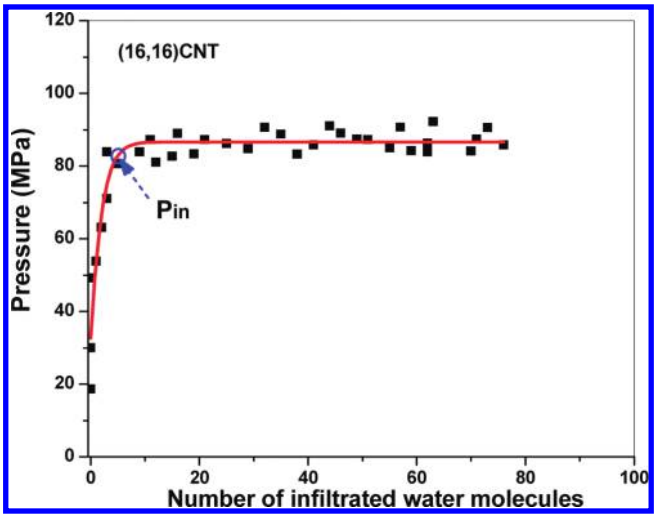

Figure 2. Reference system without applied electric field: the variation of the number of infiltrated water molecules into a (16,16) CNT as a function of applied pressure. From the plateau of the fitting curve, the critical infiltration pressure, P_{in}, can be deduced.

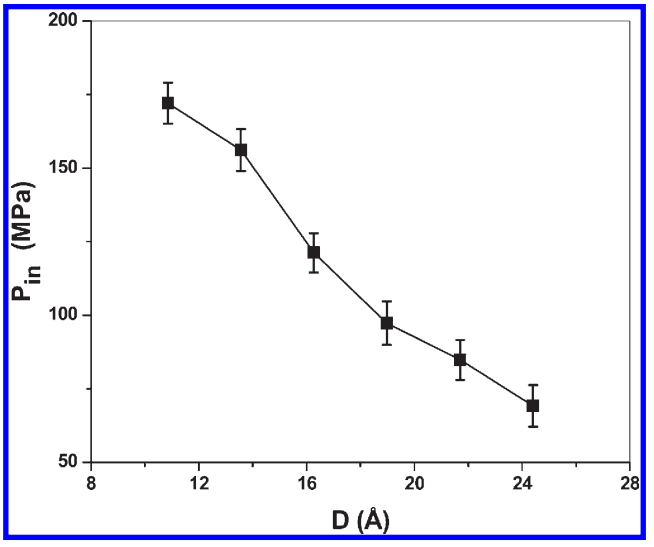

Figure 3. Effect of the CNT diameter, D, on the critical infiltration pressure, P_{in}, in the absence of external electric field. The error bar arises from the small uncertainty of determining P_{in} from the infiltration curve.

infiltrated water molecules with the applied pressure. If the pressure is relatively low, only very few water molecules are incorporated in the meniscus near the entrance of the CNT, and when the pressure exceeds a critical value of about P_{in} = 80 MPa, the capillary resistance is overcome and water molecules burst into the CNT. Afterward, the pressure remains a constant, indicating that the inner surface of the CNT is quite smooth with little transport dissipation[7] and the Laplace−Young equation can be applied at the nanoscale to correlate the infiltration pressure with solid−liquid interfacial tension.[36]

By following the similar procedure, we investigate CNTs of different chirality (diameter), from which the pore size dependence of P_{in} is given in Figure 3. The relative hydrophobicity decreases as the size of CNT gets larger with weaker solid−liquid interaction. It is important to note that the relationship between the critical infiltration pressure and pore diameter does not follow

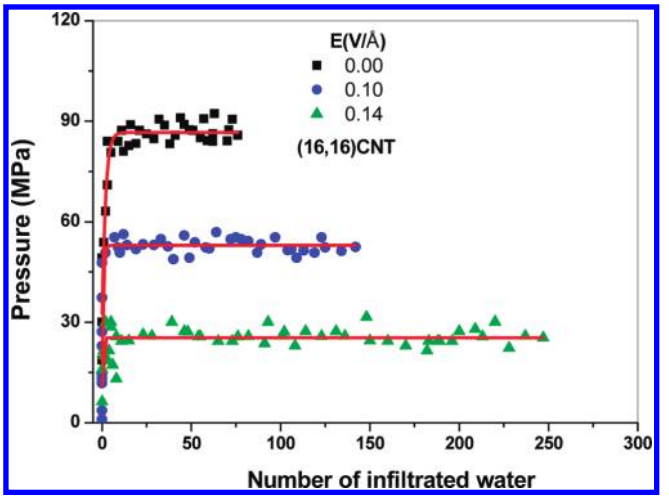

Figure 4. Effect of electric intensity on the infiltration behavior for a (16,16)CNT/water system.

the $1/D$ dependence dictated by the classic Laplace-Young equation, which indicates the strong size dependence of other involved parameters, such as the surface tension and contact angle (see below). The size dependence is further coupled with the effect of applied electric field, explored next.

Effect of Electric Field on Infiltration Characteristics in CNT/Water System. With an applied electric field, the infiltration isotherm of the water-(16,16) CNT reference system is distinct. Figure 4 indicates that more water molecules can easily enter the CNT (at lower P_{in}) with the increase of electric field, as the system becomes effectively less hydrophobic. An interesting phenomenon can be found when the direction of the electric field is switched. In Figure 5a, when $|E|$ = 0.06 V/Å, there is a small asymmetry for positive and negative electric intensities, where the P_{in} of a small (10,10) CNT is slightly smaller (and the system is a bit less hydrophobic) upon a positive electric intensity than that with a negative electric intensity. Such a nanoconfinement-induced asymmetry is more obvious if the magnitude of the applied electric intensity is increased to $|E|$ = 0.1 V/Å, Figure 5b. If the CNT gets larger, such as (18,18), then in case of a small magnitude of electric intensity (0.06 V/Å), the difference between the positive and negative electric intensity is negligible (Figure 6a); when $|E|$ is increased to 0.1 V/Å the asymmetry is apparent (Figure 6b) but the difference in infiltration behavior is still less prominent than that in the smaller (10,10) CNT.

Figure 7 plots the effect of electric field on P_{in} for six different CNT radii. It is readily seen that the P_{in} decreases with the increase of electric intensity. The asymmetry in positive and negative electric field is more obvious if the electric field is stronger, or when the CNT is smaller, and the system is slightly more nonwetting (with a higher P_{in}) in the presence of a negative electric field. These features are consistent with parallel experiment discussed below.

The underlying mechanism for electric field-dependent infiltration behavior is attributed to the inherent physical characteristics of solid−liquid interaction, such as the contact angle, surface tension, and density profile of confined liquid molecules, which are influenced by not only the electric field but also the size of the nanopore, elaborated in the next section.

Underlying Molecular Mechanism. At the equilibrium of infiltration process, with respect to the classic Laplace−Young

dx.doi.org/10.1021/la200477y |*Langmuir* 2011, 27, 6349–6357

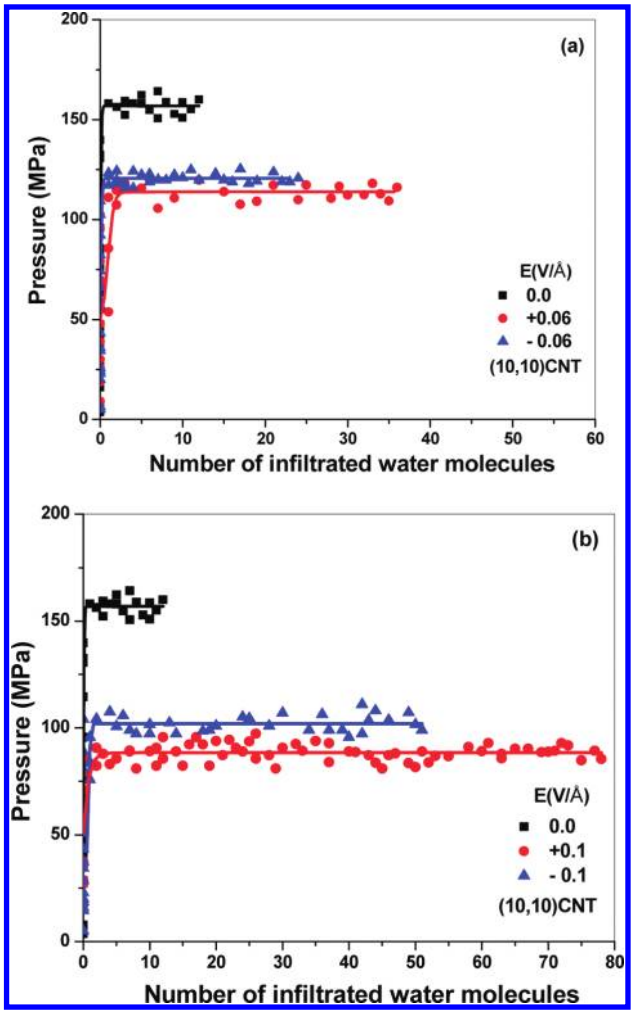

Figure 5. Effect of the direction of the external electric field on the infiltration characteristic of water molecules into a (10,10) CNT. Key: (a) ± 0.06 V/ Å and (b) ± 0.1 V/ Å.

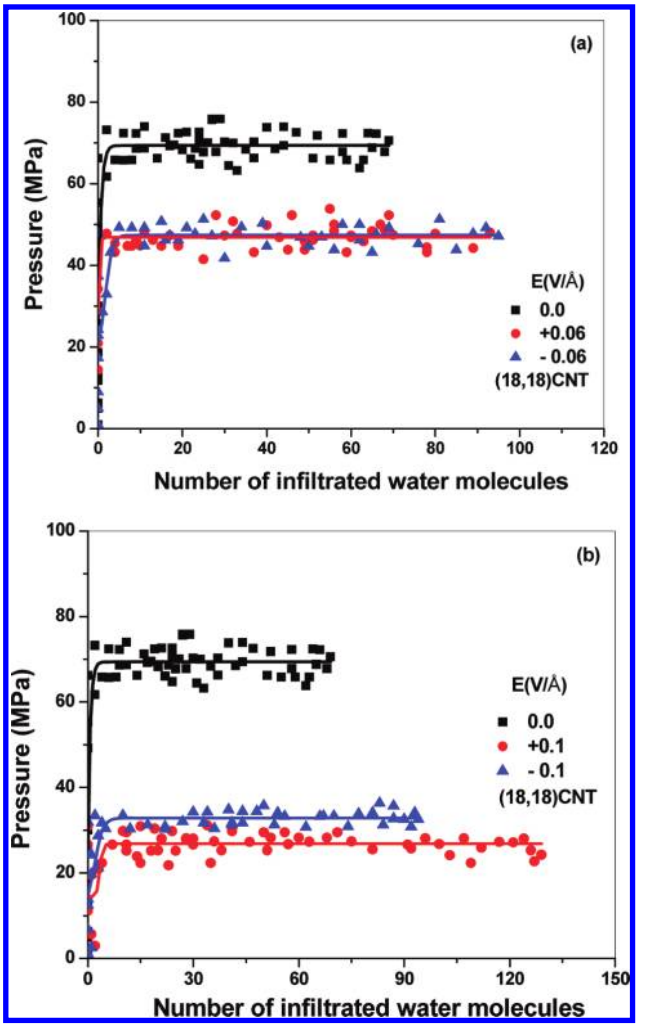

Figure 6. Effect of the direction of the external electric field on the infiltration characteristic of water molecules into a (18,18) CNT. Key: (a) ± 0.06 V/ Å and (b) ± 0.1 V/ Å.

equation, $P_{in} = -4\gamma\ [\cos\ \theta]/D$, where γ is the surface tension between water molecules inside CNT and vapor (vacuum in this study), θ is the contact angle, and D is the effective (accessible) diameter of water molecules inside the nanopore. The applicability of the Laplace−Young equation at the nanoscale has been validated,[36] as long as the relevant physical parameters (e.g., γ and θ) incorporate size effects. In this section, we focus on the effect of electric field on γ, θ, and D (as well as its coupling with the size effect), first qualitatively and then quantitatively.

First, in the absence of an external electric field (i.e., the reference system where γ=γ_0, θ=θ_0, and D=D_0), the fact that a lager nanopore diameter results in a lower P_{in} is qualitatively consistent with Figure 3, except that as remarked earlier, P_{in} does not vary as $1/D$ in Figure 3. This indicates that at the nanoscale, both surface tension and contact angle are size-dependent. That is, the curvature of nanochannel affects the configuration of confined liquid molecules, and hence both θ_0 and γ_0 depend on D. For the water−CNT system discussed herein, the overall effect is that the more constriction of water molecules in a smaller CNT subjects a stronger solid−liquid interaction, which leads to a lower θ_0 and a higher γ_0.[37]

When an external electric field is applied, according to the insight from classic electrochemistry theory, $\gamma \cos \theta = \gamma_0 \cos \theta_0 - C\phi^2/2$, where C is the interfacial capacity, and ϕ is the applied potential difference.[13] This equation indicates that regardless of the sign of the applied voltage, the effective interfacial tension $\gamma \cos \theta$ always decreases with the magnitude of ϕ, and that would reduce the critical infiltration pressure, P_{in}; these observations are qualitatively consistent with MD simulation results (Figure 7). Meanwhile, the classic theories cannot directly explain the size dependence of infiltration behavior (and its coupling with electric field dependence) and the asymmetry of positive and negative electric fields.

In order to quantify the molecular mechanism of water−carbon interaction in the nanoconfinement, two different model nanochannels, (10,10) and (18,18) CNTs, are chosen as representative cavities for accommodating water molecules. Figure 8 shows the density profile of water, $\rho(r)$, along the radial direction of a (10,10) CNT at the equilibrium after the water molecules have intruded the nanopore. The fluctuation of density profile is due to the hydrophobic nature of the considered nanotube, where most of the water molecules are confined in concentric rings/layers inside the tube; the similar characteristic of water distribution in CNTs has also been observed in other previous MD studies.[2,12,38,39]

dx.doi.org/10.1021/la200477y |*Langmuir* 2011, 27, 6349–6357

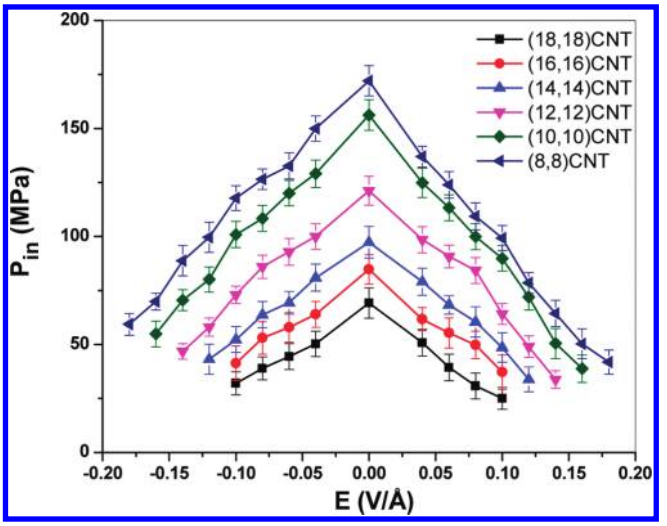

Figure 7. Coupled effect of pore size and electric field strength on the critical infiltration pressure, P_{in}.

From Figure 8, under the applied electric field, the fluctuation amplitude of the density profile decreases; moreover, the difference of the density profile under the negative and positive electric fields indicates that the wetting properties are different. These features echo the above MD simulation results. Figure 9 shows the radial density profile of water molecules confined in the larger (18,18) CNT: it can be seen that the water structure contains more concentric layers with smaller amplitude (density) than that in the (10,10) CNT, and the smaller fluctuations in the density profile suggest a weaker solid−liquid interaction and thus less sensitivity to the external electric field (as well as the asymmetry of positive and negative electric fields). With further increase of CNT diameter, it is envisioned that the radial density profile distribution will become homogeneous and deduces to that of the classic fluid behavior.

Another important feature that can be obtained from the radial density profile is the position of the first solvation shell (FSS). In the absence of the external electric field, the distances from FSS to the nanotube wall (referred as the equilibrium distance here) are 2.280 and 2.305 Å for (10,10) and (18,18) CNTs, respectively. Both of them are close to the measured value of water drop on a graphene (2.5 Å),[40,41] and the small difference is resulted from the curvature confinement effect.[37,42] With the increase of the applied electric intensity, Figures 8 and 9 indicate that the position of FSS moves away from the nanotube axis, and reduces the equilibrium distance. This is consistent with the electrowetting characteristic of water on a grapheme observed by Daub et al.[43] For a given nanotube, a smaller equilibrium distance implies a larger effective diameter D, and according to the Laplace−Young equation, that is another factor contributing to the reduction of P_{in} for the system under electric field.

Besides the effective pore size D, the surface tension γ and contact angle θ affect the infiltration behavior in a more profound manner. We first deduce the quantitative information on θ through an independent analysis. Following the technique proposed by Werder et al.,[37] for water molecules confined in a given CNT, at the equilibrium state the spatial positions of the molecules at the meniscus front are averaged in a long computational time frame, and from that averaged meniscus profile, the contact angle is deduced, illustrated in Figure 10(a) for the example of

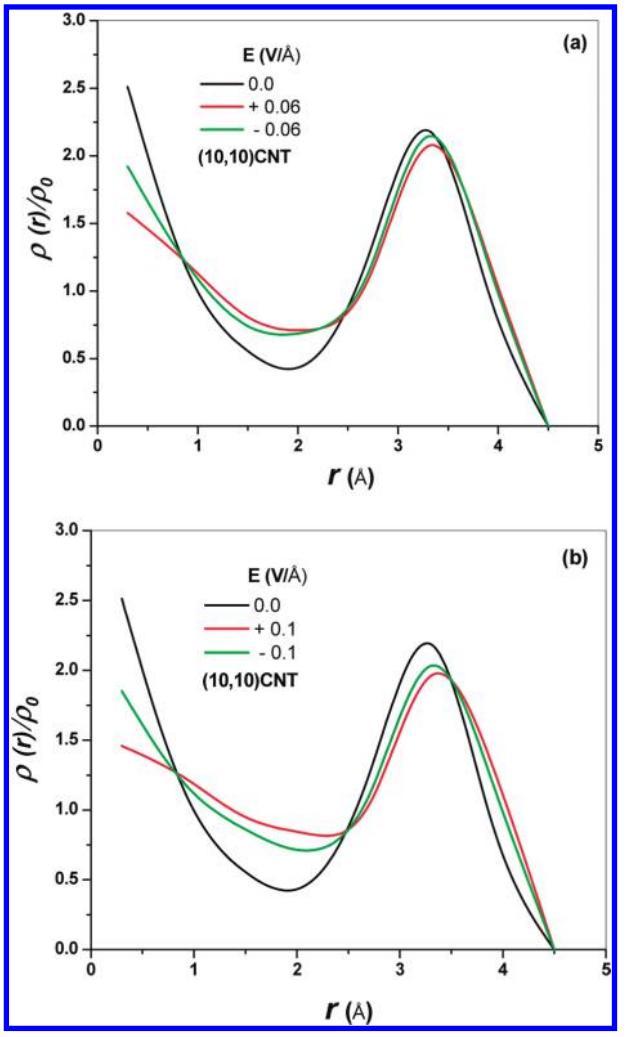

Figure 8. Normalized radial density profile of water, $\rho(r)/\rho_0$, confined in a (10,10) CNT where $\rho_0 = 998.0$ kg/m^3. Key: (a) $E = \pm 0.06$ V/Å and (b) $E = \pm 0.10$ V/Å. The left axis is aligned with the tube axis.

(18,18) CNT subjecting to an electric intensity of 0.1 V/Å. In Figure 10(b) θ is presented as a function of electric strength, and the coupled pore size effect is also shown. For (10,10) and (18,18) CNTs, the contact angle θ_o is 106.6° and 112.4°, respectively, in the absence of electric field, consistent with the hydrophobic nature. With an applied electric field, the contact angle θ decreases, and such a reduction of hydrophobicity is also larger for positive electric strength than the negative one, consistent with the trend in P_{in} (Figure 7). The anisotropy in water molecule response to the direction of an applied electric field indicates possible new electrochemistry mechanisms in a confining nanoenvironment.

Finally, based on the Laplace−Young equation, $P_{in} = -4\gamma \cos\theta/D$ and Figure 10(b), the electric field-dependent and size-dependent γ can be calculated in Figure 10(c), where the variation and dependence of D are taken into account. It can be seen that the surface tension of water in the (18, 18) CNT is ~0.11 N/m without electric field, and it increases with the reduction of CNT diameter due to the effect of CNT curvature and density of confined water molecules.[44,45] The result is consistent with that of MD results of 0.1269 N/m[46] on the water−carbon system at 300 K. Like the contact angle, the surface tension also decreases with the external

dx.doi.org/10.1021/la200477y |*Langmuir* 2011, 27, 6349–6357

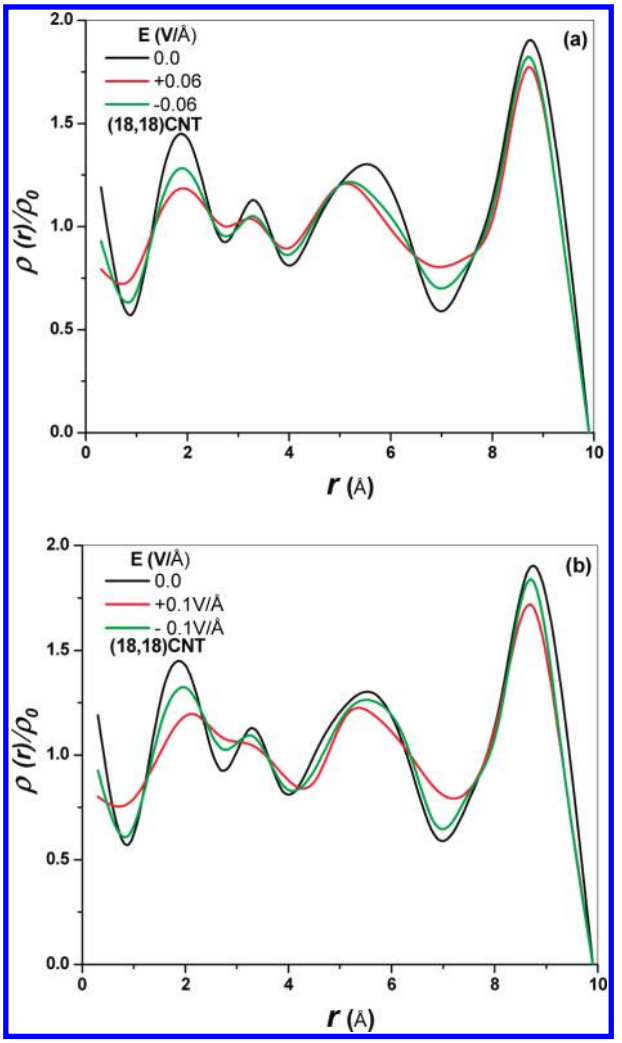

Figure 9. Normalized radial density profile of water, $\rho(r)/\rho_0$, confined in a (18,18) CNT where $\rho_0 = 998.0$ kg/m^3. Key: (a) $E = \pm 0.06$ V/Å and (b) $E = \pm 0.10$ V/Å. The left axis is aligned with the tube axis.

electric intensity. The field-induced reduction of both γ and θ contribute to the decrease of hydrophobicity (reduction of P_{in}) in the electrically controlled NEAS. The variation trend of surface tension and contact angle with respect to the applied electric field also agrees with the experiment for a water droplet resting on a graphene,[43] yet we note that in the present study, the electric field effect is closely coupled with the pore size effect.

Extend to Other Nanopores and Liquid Phases. In previous sections based on a model CNT/water system, we have revealed some basic mechanisms of the effect of electric field on infiltration behaviors. Apparently, with different solid phase and liquid composition, the infiltration characteristics are distinct. For example, in the absence of electric field, the infiltration pressure may be favorably elevated through the introduction of electrolyte as well as using silica nanotube.[30,47,48]

To demonstrate the influence of electric field on other systems, a silica nanotube (SNT) with pore size very close to that of (18,18) CNT and aqueous solution of sodium chloride (NaCl) (with molar concentration of 2.0 mol/L) are chosen as substitutes of the solid pore and liquid phase, respectively. Here the diameter of the (18,18) SNT (24.56 Å) is measured as the distance between two opposite oxygen atoms.

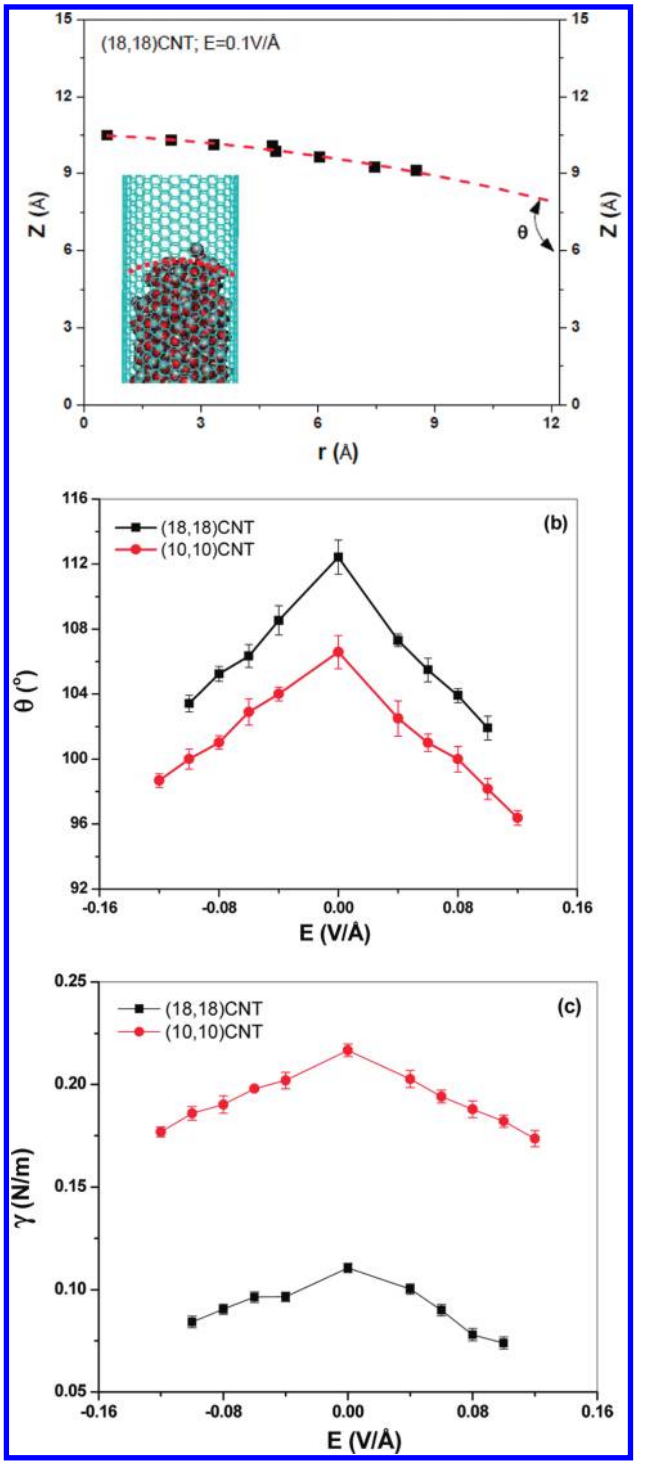

Figure 10. (a) Illustration of determining the contact angle in a (18,18) CNT upon an external electric intensity of 0.1 V/ Å; the left axis is aligned with the tube axis, and the right axis is at the tube surface. The red dash line indicates the statistically averaged spatial positions of the water molecule front in the CNT, based on which the contact angle is determined. (b) Variation of the contact angle, θ, with the external electric intensity. (c) Variation of the surface tension, γ, with electric intensity.

Following the same computational procedure above, Figure 11a plots the effect of the external electric field on P_{in}. In comparison to the CNT/water system under the same electric intensity, with

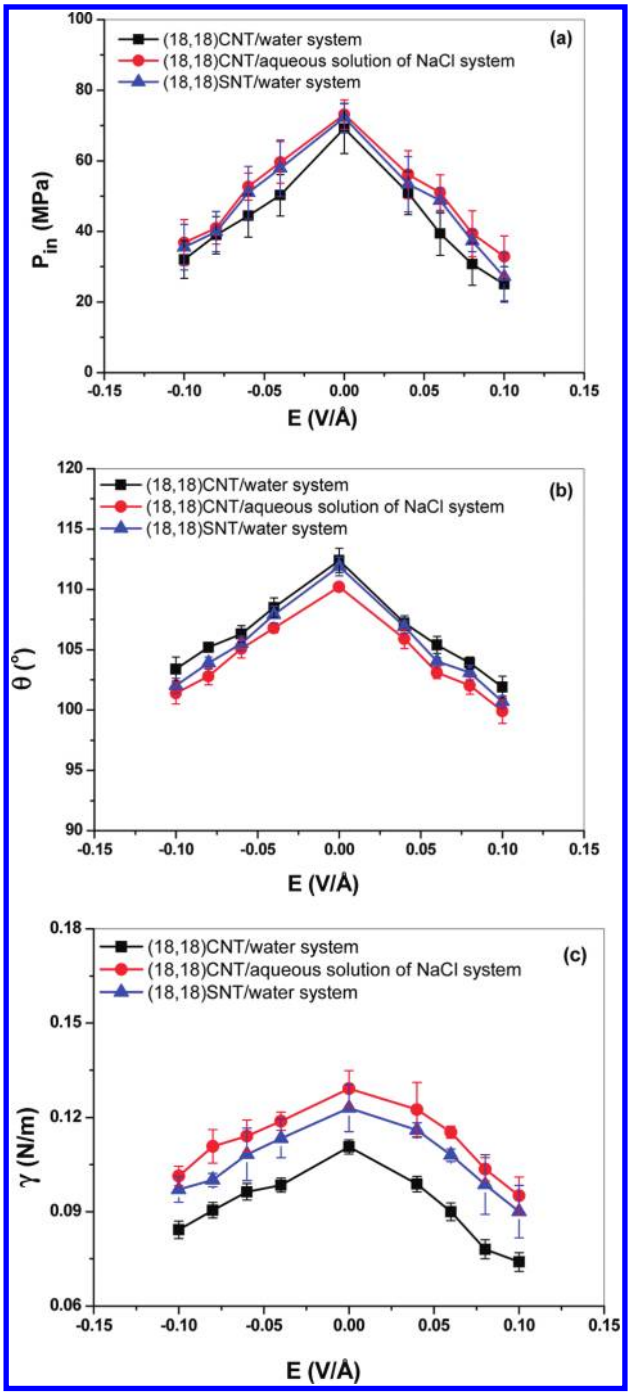

Figure 11. Comparison of different solid and liquid phases; the effect of external electric intensity on the (a) critical infiltration pressure, P_{in}, (b) contact angle, θ, and (c) surface tension, γ.

the employment of SNT or aqueous solution of NaCl, the system becomes more hydrophobic with a higher P_{in}, with the electrolyte have a bigger impact. The corresponding contact angle, θ, and surface tension, γ, are plotted in Figure 11, parts b and c, respectively: the results indicate that the increment of surface tension is mainly responsible for enhancing the hydrophobicity when the liquid/solid phases are changed. In case of the employment of electrolyte (in comparison with that of pure water), the additional work required to break the hydration shell for liquid infiltration makes P_{in} higher;[11] with an applied electric field,

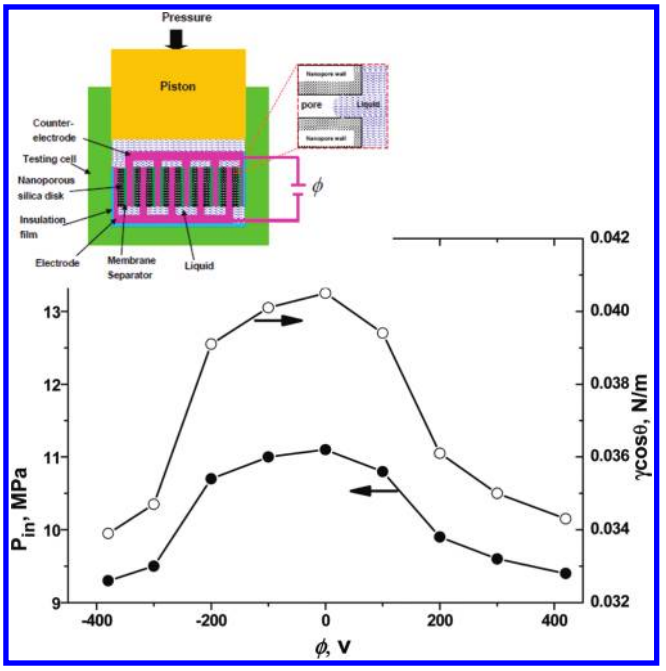

Figure 12. Experimental result on a nanoporous silica/aqueous solution of potassium chloride(KCl) system. The infiltration pressure, P_{in}, and the deduced solid−liquid interfacial tension, $\gamma \cos \theta$, in response to the applied external voltage, ϕ. The experimental setup is given in inset.

the cations and anions tend to move toward different directions and that is added to the electric strength-dependent infiltration barrier. In case where the SNT is used, the partially charged surface has a stronger interaction with the polar water molecule and that could lead to a stronger solid/liquid interfacial tension,[30] which is also sensitive to the electric field. These findings could improve the energy absorption efficiency of NEAS.

COMPARISON WITH EXPERIMENTAL DATA

The simulation results are qualitatively compared with the data of a pressure induced infiltration experiment. The nanoporous material under investigation was a nanoporous silica crystal, which was surface treated to increase the degree of hydrophobicity of the inner surfaces of nanopores.[49,50] The nanopores were confirmed to be open through a gas absorption analysis by using a Micromeritics Tristar-3000 Analyzer; the average pore diameter was about 14.6 nm. An aluminum foil was repeatedly folded to form aluminum layers, and treated silica disks of about 16.5 mg were inserted between the adjacent layers (Figure 12). The extra aluminum layers were connected together, forming an electrode and counter-electrode, respectively. The silica disks and the electrode were insulated by porous Teflon membranes, and thus a nanoporous layer stack is formed. This stack was placed at the bottom of a steel cylinder, inside which 10 g of 15% aqueous solution of potassium chloride (KCl) was sealed by another steel piston from the top. The inner surface of the cylinder was insulated from the liquid phase and aluminum layers by a Teflon layer. By using a direct current (dc) power source, an open-circuit voltage, ϕ, was applied between the lower and a counter-electrode, which was separated from the silica-aluminum layer stack by a porous polystyrene membrane. The value of ϕ was in the range −380 to +420 V. By using an Instron machine, the piston was intruded into the cylinder at a constant rate of

dx.doi.org/10.1021/la200477y |*Langmuir* 2011, 27, 6349–6357

0.5 mm/min (the loading rate was confirmed to be sufficiently slow so as not to introduce any rate effect). Since the nanopore inner surfaces were hydrophobic, only when the applied pressure was sufficiently high (beyond P_{in}) a large number of water molecules could be forced into the nanopores.

The measured P_{in} as well as the deduced effective interfacial tension are given in Figure 12 as a function of the applied voltage, where the trend is qualitatively consistent with the computational results (Figures 7 and 10), suggesting that P_{in} decreases with increasing $|E|$, despite the difference between the experimental and simulation systems. In addition, the direction of the electric field has some effect on P_{in}, and a lower P_{in} is observed in the presence of the positive electric field, which is also consistent with predictions in Figure 7. All these phenomena again suggest that the conventional electrochemistry theory should be enriched the nanoscale.

Note that the current agreement between simulation and experiment is rather qualitative, owing to several practical challenges that have not yet been overcome. First, the experimental system is much larger than the simulation cell, with the pore size larger and length longer. Second, the diameter of nanopores in the experimental systems is not quite uniform, and the pore structure is also quite complex. Third, the surface treatment used in experiment is difficult to incorporate into simulation. Last but not least, due to the size and time scale accessible to MD simulation, the electrical strength applied in simulation is much higher than that in experiment. A more quantitative coordination between simulation and experiment will be reported in future.

CONCLUDING REMARKS

By taking advantage of the large specific surface area of nanoporous materials, a number of nanofluidic devices have been proposed whose functionality critically depends on the ability to control the effective solid−liquid interfacial tension. In this paper, we investigate the possibility of adjusting the liquid−solid interactions by using electric field, and explore the electric strength-dependent infiltration behaviors of water molecules into hydrophobic nanopores. Systematic MD simulations of CNT/water systems show that the critical infiltration pressure reduces with the increase of electric intensity or pore size. The factors contributing to the reduced hydrophobicity include the electrical induced variations of surface tension and contact angle, as well as radial density profile of confined liquid molecules. An interesting phenomenon of asymmetric response to positive and negative electric fields is discovered, which is associated with the asymmetry in radial density profile and contact angle. The coupling between the electric field effect and pore size effect is elucidated, as well as the effect of using electrolyte and polar nanopore. These unique nanoscale characteristics provide insights for the variation of the effective interfacial tension, which are qualitatively validated by using a parallel experiment, and similar trends of electric field dependencies are found.

The critical influence of the electrical field on the nanofluidic behavior is expected to facilitate the development of high efficiency nanodevices. For example, on the basis of electrically controlled switching of relative wetting/dewetting of nanopores, a nanoporous electric machine may be developed. Consider a nanoporous material that is soaked in a liquid, a constant pressure may be applied which is bounded by the infiltration pressure levels at different electric fields; thus, with the change of electric field, the relative hydrophobicity is varied and the liquid may spontaneously infiltrate the nanopores at a larger electric strength, which reduces the system volume and outputs mechanical work. The potential output of such a system may be estimated as the effective solid−liquid interfacial tension times the surface area of nanopore, which may reach the order of 100 J/g and thus orders of magnitude higher than conventional smart systems (e.g., piezoelectrics). The reduction of the infiltration threshold under electric field may also be used to fine-tune the energy absorption performance of the nanoporous solid/liquid composite. And the working mechanisms of these nanodevices will be underpinned by the unveiled principles of interactions between the nanoconfined liquid molecules and solid pore/channel, which may be further enriched in future by incorporating the effects of temperature, pore surface structures, and surface treatments, among others.

AUTHOR INFORMATION

Corresponding Authors

*E-mail: xichen@columbia.edu (Xi Chen) and qlzhou@mail.xjtu.edu.cn (Qulan Zhou). Columbia Nanomechanics Research Center, Department of Earth and Environmental Engineering, Columbia University, New York, New York 10027, United States.

ACKNOWLEDGMENT

The work is supported by National Natural Science Foundation of China (50928601), World Class University program through the National Research Foundation of Korea (R32−2008−000−20042−0), Changjiang Scholar Program from Ministry of Education of China, and National Science Foundation (CMMI-0643726).

REFERENCES

(1) Helmy, R.; Kazakevich, Y.; Ni, C.; Fadeev, A. Y. *J. Am. Chem. Soc.* **2005**, *127*, 12446–12447.
(2) Hummer, G.; Rasalah, J. G.; Noworyta, J. P. *Nature* **2001**, *414*, 188–190.
(3) Sparreboom, W.; Vandenberg, A.; Eijkel, J. C. T. *Nat. Nanotech.* **2009**, *4*, 713–720.
(4) Dujardin, E.; Ebbesen, T. W.; Hiura, H.; Tanigaki, K. *Science* **1994**, *265*, 1850–1852.
(5) Zhao, J.; Culligan, P. J.; Germaine, J. T.; Chen, X. *Langmuir* **2009**, *25*, 12687–12696.
(6) Chen, X.; Surani, F. B.; Kong, X.; Punyamurtula, V. K.; Qiao, Y. *Appl. Phys. Lett.* **2006**, *89*, 241918.
(7) Chen, X.; Cao, G.; Han, A.; Punyamurtula, V. K.; Liu, L.; Culligan, P. J.; Kim, T.; Qiao, Y. *Nano Lett.* **2008**, *8*, 2988–2992.
(8) Han, A.; Qiao, Y. *Chem. Lett.* **2007**, *36*, 882–883.
(9) Qiao, Y.; Cao, G.; Chen, X. *J. Am. Chem. Soc.* **2007**, *129*, 2355–2359.
(10) Han, A.; Chen, X.; Qiao, Y. *Langmuir* **2008**, *24*, 7044–7047.
(11) Liu, L.; Chen, X.; Lu, W.; Qiao, Y. *Phys. Rev. Lett.* **2009**, *102*, 184501.
(12) Liu, L.; Zhao, J.; Culligan, P. J.; Qiao, Y.; Chen, X. *Langmuir* **2009**, *25*, 11862–11868.
(13) Lu, W.; Kim, T.; Han, A.; Chen, X.; Qiao, Y. *Langmuir* **2009**, *25*, 9463–9466.
(14) Wong-ekkabut, J.; Miettinen, M. S.; Dias, C.; Karttunen, M. *Nat. Nanotech.* **2010**, 555–557.
(15) Bonthuis, D. J.; Falk, K.; Kaplan, C. N.; Horinek, D.; Berker, A. N.; Bocquet, L.; Netz, R. R. *Phys. Rev. Lett.* **2010**, *105*, 209401.

(16) Bratko, D.; Daub, C. D.; Luzar, A. *Phys. Chem. Chem. Phys.* **2008**, *10*, 6807–6813.
(17) Bratko, D.; Daub, C. D.; Leung, K.; Luzar, A. *J. Am. Chem. Soc.* **2007**, *129*, 2504–2510.
(18) Garate, J. A.; English, N. J.; MacElroy, J. M. D. *J. Chem. Phys.* **2009**, *131*, 114508.
(19) The chirality (c,c) is used to imply the size of the employed armchair CNT in this paper, and the ratio between c and CNT diameter is fixed
(20) Zhao, J.; Liu, L.; Culligan, P. J.; Chen, X. *Phys. Rev. E* **2009**, *80*, 061206.
(21) Plimpton, S. *J. Comput. Phys.* **1995**, *117*, 1–19.
(22) http://lammps.sandia.gov.
(23) Zhu, S. B.; Yao, S.; Zhu, J. B.; Singh, S.; Robinson, G. W. *J. Phys. Chem. B* **1991**, *95*, 6211–6217.
(24) The effect of flexibility of water on infiltration depends on the intramolecular potential. For example, if the stretching of OH bond is modeled by the Morse potential, it will lead to a "softening" of the intermolecular potential and thus will decrease the critical infiltration pressure; meanwhile, if the harmonic potential is employed, it is expected to increase the infiltration pressure.
(25) Berendsen, H. J. C.; Grigera, J. R.; Straatsma, T. P. *J. Phys. Chem.* **1987**, *24*, 6269–6271.
(26) Werder, T.; Walther, J. H.; Jaffe, R. L.; Halicioglu, T.; Koumoutsakos, P. *J. Phys. Chem. B* **2003**, *107*, 1345–1352.
(27) The van der Waals parameters between water and CNT will affect the threshold pressure. In the present study, we employ the most popular L-J parameters which have been proved to reproduce the experimental results in literature.
(28) Werder, T.; Walther, J. H.; Jaffe, R. L.; Halicioglu, T.; Koumoutsakos, P. *J. Phys. Chem. B* **2003**, *107* (6), 1345–1352.
(29) Liu, L.; Chen, X.; Han, A.; Qiao, Y. *New J. Phys.* **2010**, *12*, 033021.
(30) Zhao, J.; Culligan, P. J.; Qiao, Y.; Zhou, Q.; Li, Y.; Tak, M.; Park, T.; Chen, X. *J. Phys.: Condens. Matter* **2010**, *22*, 315301.
(31) During the loading process, the piston moves a small distance at each step and then is held fixed until the system reaches equilibrium
(32) Note that when a periodical boundary is used in MD simulation, the interactions across periodical boundaries can be included by considering the ghost atoms inside the computational cell, ensuring the validity of this equation
(33) Berkowitz, M. L.; Bostick, D. L.; Pandit, S. *Chem. Rev.* **2006**, *106*, 1527–1539.
(34) Philippsen, A.; Im, W.; Engel, A.; Schirmer., T.; Roux, R.; Muller, D. J. *Biophys. J.* **2002**, *82*, 1667–1676.
(35) Vaitheeswaran, S.; Yin, H.; Rasaiah, J. C. *J. Phys. Chem. B* **2005**, *109*, 6629–6635.
(36) Liu, L.; Zhao, J.; Yin, C. Y.; Culligan, P. J.; Chen, X. *Phys. Chem. Chem. Phys.* **2009**, *11*, 6520–6524.
(37) Werder, T.; Walther, J. H.; Jaffe, R. L.; Halicioglu, T.; Noca, F.; Koumoutsakos, P. *Nano Lett.* **2001**, *1*, 697–702.
(38) Thomas, J. A.; McGaughey, A. J. H. *J. Chem. Phys.* **2008**, *128* 084715.
(39) Hanasaki, I.; Nakatani, A. *J. Chem. Phys.* **2006**, *124*, 144708.
(40) Nagy, G. *J. Electroanal. Chem.* **1996**, *409*, 19–23.
(41) Gordillo, M. C.; Martí, J. *Phys. Rev. B* **2008**, *78*, 075432.
(42) Kutana, A.; Giapis, K. P. *Phys. Rev. B* **2007**, *76*, 195444.
(43) Daub, C. D.; Bratko, D.; Leung, K.; Luzar, A. *J. Phys. Chem. C* **2007**, *111*, 505–509.
(44) Ahn, W. S.; Jhon, M. S.; Pak, H.; Chang, S. *J. Colloid Interface Sci.* **1972**, *38*, 605–608.
(45) Prylutskyy, Y. I.; Matzui, L. Y.; Gavryushenko, D. A.; Sysoev, V. M.; Scharff, P. *Fullerenes, Nanotubes, Carbon Nanostruct.* **2005**, *13*, 287–291.
(46) Walther, J. H.; Jaffe, R.; Halicioglu, T.; Koumoutsakos, P. *J. Phys. Chem. B* **2001**, *105*, 9980–9987.
(47) Cruz-Chu, E. R.; Aksimentiev, A.; Schulten, K. *J. Phys. Chem. B* **2006**, *110*, 21497–21508.
(48) Desbiens, N.; Boutin, A.; Demachy, I. *J. Phys. Chem. B* **2005**, *109*, 24071–24076.
(49) Han, A.; Qiao, Y. *Langmuir* **2007**, *23*, 11396–11398.
(50) Lim, M. H.; Stein, A. *Chem. Mater.* **1999**, *11*, 3285–3295.